BIOTECHNOLOGY

Rescue of autosomal dominant hearing loss by in vivo delivery of mini dCas13X-derived RNA base editor

Qingquan Xiao[1,2]†, Zhijiao Xu[3,4,5]†, Yuanyuan Xue[3,4,5]†, Chunlong Xu[6]†, Lei Han[3,4,5,7], Yuanhua Liu[1], Fang Wang[3,4,5], Runze Zhang[1,2], Shuang Han[3,4,5,8], Xing Wang[9], Geng-Lin Li[3,5], Huawei Li[3,4,5,10]*, Hui Yang[1]*, Yilai Shu[3,4,5]*

Programmable RNA editing tools enable the reversible correction of mutant transcripts, reducing the potential risk associated with permanent genetic changes associated with the use of DNA editing tools. However, the potential of these RNA tools to treat disease remains unknown. Here, we evaluated RNA correction therapy with Cas13-based RNA base editors in the myosin VI p.C442Y heterozygous mutation (*Myo6*$^{C442Y/+}$) mouse model that recapitulated the phenotypes of human dominant-inherited deafness. We first screened several variants of Cas13-based RNA base editors and guide RNAs (gRNAs) targeting *Myo6*^{C442Y} in cultured cells and found that mini dCas13X.1-based adenosine base editor (mxABE), composed of truncated Cas13X.1 and the RNA editing enzyme adenosine deaminase acting on RNA 2 deaminase domain variant (ADAR2dd^{E488Q}), exhibited both high efficiency of A > G conversion and low frequency of off-target edits. Single adeno-associated virus (AAV)–mediated delivery of mxABE in the cochlea corrected the mutated *Myo6*^{C442Y} to *Myo6*^{WT} allele in homozygous *Myo6*$^{C442Y/C442Y}$ mice and resulted in increased *Myo6*^{WT} allele in the injected cochlea of *Myo6*$^{C442Y/+}$ mice. The treatment rescued auditory function, including auditory brainstem response and distortion product otoacoustic emission up to 3 months after AAV-mxABE-*Myo6* injection in *Myo6*$^{C442Y/+}$ mice. We also observed increased survival rate of hair cells and decreased degeneration of hair bundle morphology in the treated compared to untreated control ears. These findings provide a proof-of-concept study for RNA editing tools as a therapeutic treatment for various semidominant forms of hearing loss and other diseases.

INTRODUCTION

Site-directed RNA editing technologies lead endogenous or exogenous deaminases by guide RNA (gRNA) or gRNA-RNA binding protein complex on target RNA loci to mediate A-to-I or C-to-U base conversion, a potential gene therapy approach for genetic diseases (*1*). Deaminases widely used by currently developed RNA base editors are adenosine deaminases acting on RNA (ADARs) including ADAR1 and ADAR2, which recognize and convert A to I on their cognate substrate of double-strand RNA such as GluR2 mRNA in mammalian cells (*2*). Inosine as catalysis product of ADARs is a deaminated form of adenosine that is biochemically recognized as guanine upon mRNA translation.

As early as the 1990s, scientists designed the artificial antisense oligonucleotides (ASOs) recruiting endogenous ADARs to successfully install A-to-I editing for the correction of a premature stop codon mutation on dystrophin RNA in *Xenopus* embryos (*3*), echoing with three recently developed methods including GluR-ADAR (*4*), RESTORE (recruiting endogenous ADAR to specific transcripts for oligonucleotide-mediated RNA editing) (*5*), and LEAPER (leveraging endogenous ADAR for programmable editing of RNA) (*6*). However, gRNA-mediated recruitment of endogenous ADARs strongly relies on the abundance and substrate specificity of ADAR family members expressed in edited cells. Recruiting endogenous ADARs also depends on the efficient creation and introduction of exogenous RNA structures that are recognized by ADARs, which might interfere with the endogenous ADAR-RNA regulation network. In addition, the method cannot be used for C-to-U and other types of RNA base editing. Meanwhile, endogenous ADAR-independent RNA editing systems, λN-ADAR (*7*–*9*) and MS2–MCP (MS2 coat protein)–ADAR (*10*, *11*), were further developed by replacing endogenous targeting domains of ADARs with λ-phage N protein and bacteriophage MCP, respectively. Cognate hairpin motif sequences for specific λN and MCP recognition were fused with guide sequence to enable site-directed A-to-I editing. However, notable off-target editing needs to be considered for λN-ADAR and MS2-MCP-ADAR (*10*–*13*). Recently, RNA-targeting CRISPR-Cas13 systems were repurposed for efficient RNA base editing exemplified by REPAIR (RNA Editing for Programmable A to I Replacement) (*14*) and RESCUE (RNA Editing for Specific C-to-U Exchange) (*15*) technologies, reviving the development of versatile RNA editing modality. REPAIR and RESCUE have shown the ability to correct genetic mutations by gRNA-programmed deaminases activity on mutant transcripts in culture cells. However, they are not suitable for in vivo delivery with a single adeno-associated virus (AAV) vector due to the large size property of PspCas13b and ADAR proteins. Therefore,

[1]Institute of Neuroscience, State Key Laboratory of Neuroscience, Key Laboratory of Primate Neurobiology, CAS Center for Excellence in Brain Science and Intelligence Technology, Shanghai Research Center for Brain Science and Brain-Inspired Intelligence, Shanghai Institutes for Biological Sciences, Chinese Academy of Sciences, Shanghai 200031, China. [2]College of Life Sciences, University of Chinese Academy of Sciences, Beijing 100049, China. [3]ENT Institute and Department of Otorhinolaryngology, Eye & ENT Hospital, State Key Laboratory of Medical Neurobiology and MOE Frontiers Center for Brain Science, Fudan University, Shanghai 200031, China. [4]Institutes of Biomedical Sciences, Fudan University, Shanghai 200032, China. [5]NHC Key Laboratory of Hearing Medicine, Fudan University, Shanghai 200032, China. [6]Lingang Laboratory, Shanghai Center for Brain Science and Brain-Inspired Intelligence Technology, Shanghai 200032, China. [7]Department of Otorhinolaryngology, Second Affiliated Hospital, University of South China, Hengyang 421001, China. [8]Department of Otolaryngology Head and Neck Surgery, Second Hospital of Jilin University, Changchun 130000, China. [9]Huigene Therapeutics Inc., Shanghai 201315, China. [10]Institutes of Brain Science and the Collaborative Innovation Center for Brain Science, Fudan University, Shanghai 200032, China.
*Corresponding author. Email: hwli@shmu.edu.cn (H.L.); huiyang@ion.ac.cn (H.Y.); yilai_shu@fudan.edu.cn (Y.S.)
†These authors contributed equally to this work.

the mini base editors derived from compact Cas13 proteins were developed and exhibited both high on-target and low off-target efficiency for A-to-I and C-to-U substitution (*16*, *17*). Because of its compact size, the mini base editor [mini dCas13X-based adenine base editor (mxABE)] provides a potential to treat genetic diseases in vivo via a single AAV vector.

Although in vivo application of λN-ADAR and MS2-MCP-ADAR showed promising editing efficacy for restoring expression of normal protein, no definitive therapeutic effect was observed (*8*, *18*). Therefore, in vivo therapeutic validity of RNA editing tools remains yet largely investigated in disease models for both RNA editing efficacy and therapeutic improvement of disease-related symptoms. Myosin VI (MYO6) is an unconventional myosin anchoring on the stereocilia and vestibular plate of hair cells in the cochlear, which is vital for auditory function (*19*). Pathogenic variants in the human MYO6 gene cause autosomal dominant or recessive forms of hearing loss with unmet need for potential therapy (*19*–*23*). The *Myo6*$^{C442Y/+}$ mouse model was established and recapitulated the phenotypes of human dominant-inherited deafness (*24*). In this study, we found that injection of AAV-PHP.eB–mxABE targeting the *Myo6*^{C442Y} RNA into the cochlea of neonatal *Myo6*$^{C442Y/+}$ mice substantially reduced progressive hearing loss. Our findings support the use of this therapeutic strategy for semidominant diseases and potentially for recessive diseases.

RESULTS

Screen of different RNA base editors and gRNAs for *Myo6*^{C442Y} correction

The *Myo6*$^{C442Y/+}$ mice have a G-to-A change (NM_001039546.1: c.1325G > A), and we thus aimed to induce A-to-G conversion in *Myo6*^{C442Y} RNA by adenine RNA base editors. To establish the in vitro readout of *Myo6*^{C442Y} correction efficiency, we fused mutant *Myo6*^{C442Y} with *mCherry* via *P2A* sequence to overexpress *Myo6*^{C442Y} RNA in human embryonic kidney (HEK) 293T cells (Fig. 1A), cotransfected with different RNA base editors and gRNAs targeting C442Y mutation (Fig. 1A and fig. S1). In the screening, our recently reported mini A-to-I base editor, mxABE (*16*), derived from the truncated Cas13X fusion with ADAR2, was smaller compared with the commonly used REPAIR system derived from Cas13b (Fig. 1B) (*14*). Furthermore, we fused truncated Cas13X or Cas13b with two versions of ADAR2 deaminase domain (ADAR2dd) carrying different mutations: ADAR2dd^{E488Q} (v1) for high activity (*16*) and ADAR2dd$^{E488Q/T375G}$ (v2) for high fidelity of base editing (*16*). In addition, we also examined the effect of mismatched base position within a 50–nucleotide spacer on A-to-I editing efficiency for both mxABE-v1/v2 and REPAIR-v1/v2 (fig. S1, A and B). The base editing activity of mxABE-v1/v2 and REPAIR-v1/v2 was evaluated by targeted deep sequencing of *mCherry-Myo6*^{C442Y} fusion RNA in green fluorescent protein–positive (GFP$^+$)/mCherry$^+$ cells. We found comparable editing efficiency between mxABE-v1 (65.84 ± 1.04%) and REPAIR-v1 (59.21 ± 0.81%); both showed higher base editing efficiency than mxABE-v2 (44.67 ± 0.51%) and REPAIR-v2 (39.71 ± 1.81%) (Fig. 1C). In addition, gRNAs carrying mismatch nucleotide against C442Y mutation on different positions showed slightly variable efficiency, with the highest A-to-I conversion rate on position A28 and A35 for mxABE-v1/v2 and REPAIR-v1/v2, respectively (Fig. 1C).

To investigate off-target effects of *Myo6*^{C442Y}-targeting base editors, we performed transcriptome-wide RNA sequencing (RNA-seq) analysis on mxABE, REPAIR, or ADAR2dd variants in HEK293T cells (fig. S1C) and found that REPAIR-v2 generated substantial off-target A-to-I editing events at the transcriptomic scale (Fig. 1, D and E). By contrast, both mxABE-v1 and mxABE-v2 showed much lower off-target edits than REPAIR-v2 (Fig. 1, D and E). Cells treated with ADARdd-v1 carried higher off-target edits than cells treated only with ADARdd-v2, and those off-target edits induced by ADARdd-v1 were reduced by fusing ADARdd-v1 with truncated Cas13X (mxABE-v1). Considering high editing efficiency, low off-target edits, and small size (830 amino acids in total), we selected mxABE-v1 for the following in vivo experiments in the *Myo6*^{C442Y} mouse model.

In vivo correction of *Myo6*^{C442Y} with mxABE

To verify the in vivo activity of mxABE against C442Y mutation, we packaged mxABE-v1– and gRNA-targeting C442Y mutation with mismatch on A26 (hereafter referred to as mxABE-T) into AAV-PHP.eB (Fig. 2A), an AAV variant infecting hair cells with high efficiency (*25*). The AAV-PHP.eB–mxABE-T was injected into the right inner ear of *Myo6*$^{C442Y/+}$ and *Myo6*$^{C442Y/C442Y}$ mice post-natal day 0 (P0) to P2, whereas the left ear remained uninjected (Fig. 2B). Two or more weeks after injection, the inner ear was dissected from both uninjected and injected cochlea of the same mouse to analyze A-to-I editing efficiency of AAV-PHP.eB–mxABE-T. For heterozygous *Myo6*$^{C442Y/+}$ mice, Sanger sequencing results revealed an increase of G base for wild type (WT) (*Myo6*$^+$ or WT) versus A base for mutant allele (*Myo6*^{C442Y}) when a pair of mxABE-T–injected and uninjected ear was analyzed (Fig. 2C and fig. S2A). We further confirmed these results by deep sequencing and found up to 2.01-fold (1.48-fold in average) increase of WT (*Myo6*$^+$) allele after AAV-PHP.eB–mxABE-T injection in *Myo6*$^{C442Y/+}$ mice (Fig. 2D and fig. S2A). In vivo–targeted deep sequencing data showed no substantial bystander off-target edits around the target site (fig. S2A). We also found that there was no significant change of WT allele between the left and right cochlea of *Myo6*$^{C442Y/+}$ mice without treatment, further supporting the notion that the increase of WT allele in treated mice was induced by mxABE-T injection (fig. S2, B to D). Furthermore, the G-to-A ratio calculated by sequencing of *Myo6* transcript from untreated *Myo6*$^{C442Y/+}$ mice was close to 50% (Fig. 2, C and D, and fig. S2, A, C, and D). We also injected AAV-PHP.eB–mxABE-T into *Myo6*$^{C442Y/C442Y}$ mice and found 4.22 ± 0.68% editing efficiency (Fig. 2E), suggesting partial correction of mutant (*Myo6*^{C442Y}) to WT (*Myo6*$^+$) allele by RNA base editing.

To further confirm the editing specificity of mxABE, we also packaged mxABE with nontarget gRNA into AAV-PHP.eB and injected the virus into the right inner ear of *Myo6*$^{C442Y/+}$ mice. Sanger sequencing trace data exhibited no detectable editing events (fig. S3A). To assess virus expression, we conducted quantitative reverse transcription polymerase chain reaction (qRT-PCR) to quantify mxABE expression showing the injected ears with high mxABE expression compared with ears of untreated mice [expression of mxABE calculated by the ΔΔ*C*t (cycle threshold) method, untreated *Myo6*$^{C442Y/+}$ mice: left ears, 1.39 ± 0.17; right ears, 0.76 ± 0.04; mxABE-treated *Myo6*$^{C442Y/+}$ mice: left ears, 157.50 ± 69.31; right ears, 3334.00 ± 767.20] (fig. S3B). In addition, we found high expression of mxABE in injected right ears but low expression of mxABE in uninjected left ears of treated mice in contrast to no expression of mxABE at all in both ears of untreated mice, indicating that a small amount of virus in some right ear–injected *Myo6*$^{C442Y/+}$ mice might traffic from right (injected) ears to the left (uninjected) ones (fig.

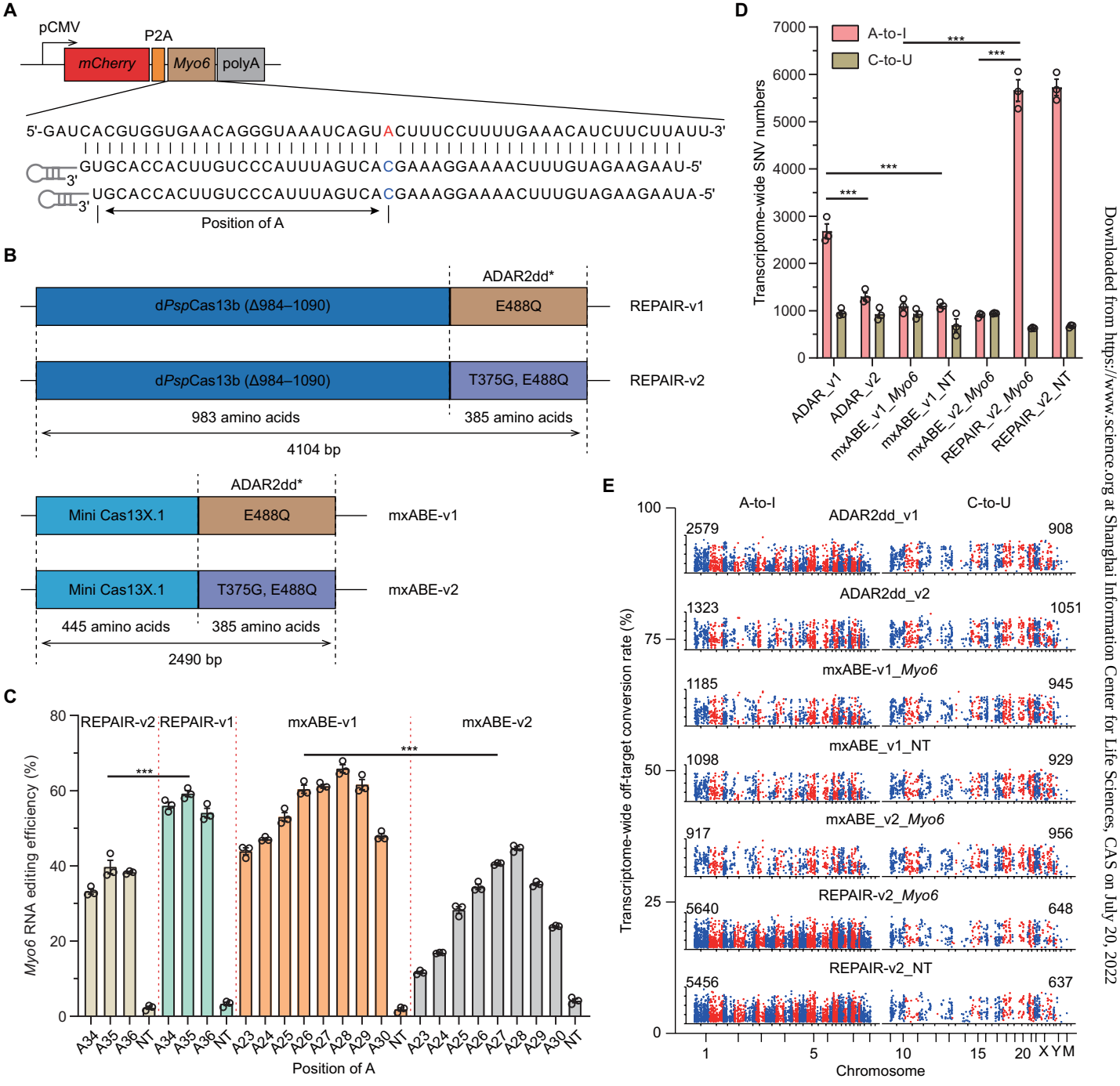

Fig. 1. Screen of RNA base editors and gRNAs for efficiently correcting *Myo6*^{C442Y} mutation. (**A**) Diagram of reporter gene *mCherry-P2A-Myo6*^{C442Y} for base editors screening in HEK293T cells. The blue capital C indicates mismatched base against A mutation in *Myo6* transcript. pCMV, porcine cytomegalovirus. (**B**) Schematic design and size of different base editors. (**C**) Effect of mismatch base position on A-to-I conversion rate achieved by different base editors. NT, nontarget gRNA. mxABE-v1 versus mxABE-v2, $P < 0.001$, Student's *t* test; REPAIR-v1 versus REPAIR-v2, $P < 0.001$, Student's *t* test. Mismatch positions comparison for mxABE-v1, $P < 0.001$, one-way ANOVA and for REPAIR-v1, $P < 0.05$, one-way ANOVA. (**D**) Total single-nucleotide variants (SNVs) of A-to-I and C-to-U at transcriptome wide identified as off-target editing events for different base editors. mxABE-v1 versus REPAIR-v2, $P < 0.001$, Student's *t* test; mxABE-v2 versus REPAIR-v2, $P < 0.001$, Student's *t* test; ADAR-v1 versus ADAR-v2, $P < 0.001$, Student's *t* test; mxABE-v1-NT versus ADAR-v1, $P < 0.001$, Student's *t* test. (**E**) Transcriptomic distribution of off-target editing events induced by different base editors. The *x* axis indicates chromosomes, and the *y* axis denotes the off-target activity. Data are presented as means ± SEM. *$P < 0.05$ and ***$P < 0.001$

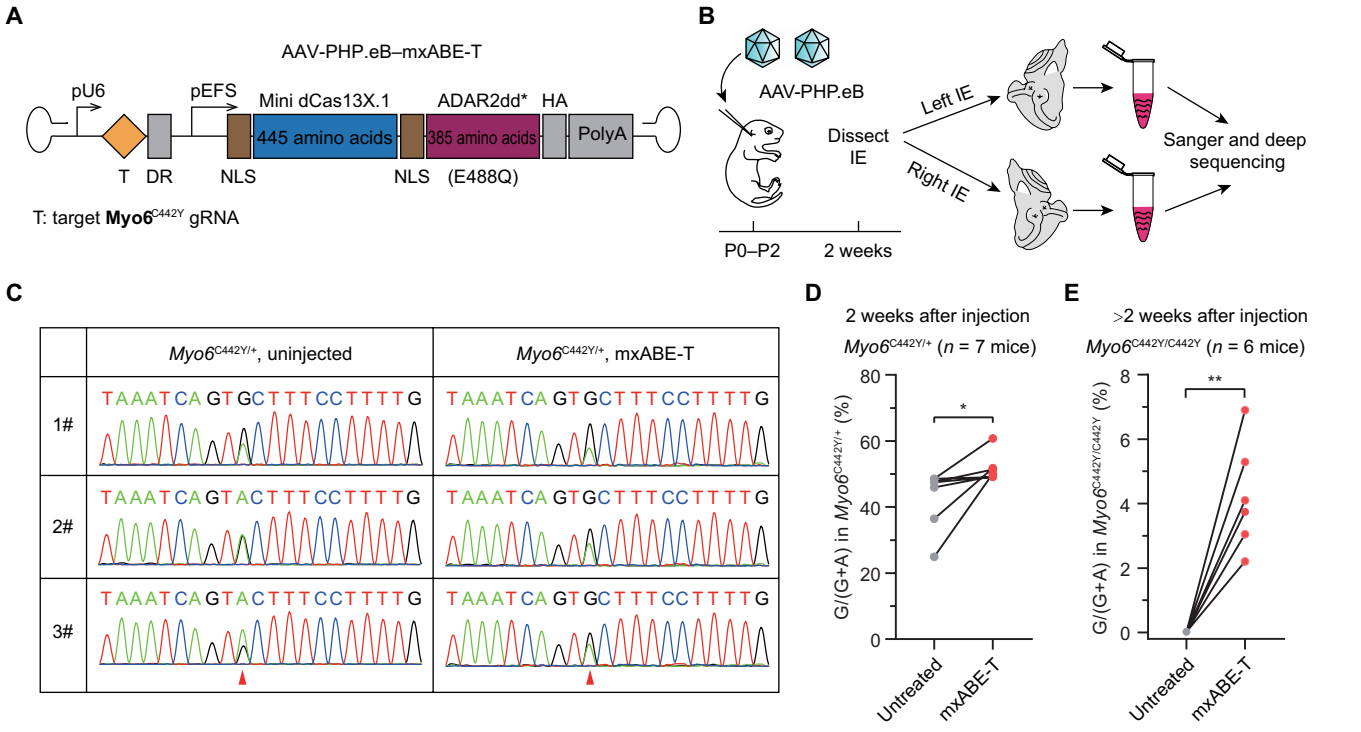

Fig. 2. In vivo correction of *Myo6*^{C442Y} mutation with mxABE delivered by AAV-PHP.eB. (**A**) Schematic design of AAV carrying mxABE-targeting *Myo6*^{C442Y} mutation. HA, hemagglutinin; NLS, nuclear localization signal; DR, direct repeat; pEFS, EF1 alpha promoter short form. (**B**) The workflow for in vivo delivery of *Myo6*^{C442Y}-targeting AAV-mxABE and activity verification in the cochlea of *Myo6*$^{C442Y/C442Y}$ and *Myo6*$^{C442Y/+}$ mice 2 weeks after injection. IE, inner ear. (**C**) Sanger sequencing results for in vivo correction of *Myo6*^{C442Y} mutation in the cochlea of *Myo6*$^{C442Y/+}$ mice injected with AAV-mxABE and the corresponding uninjected cochlea, with red arrowheads indicating the target nucleotide. (**D**) Deep sequencing results in the cochlea of *Myo6*$^{C442Y/+}$ mice injected with AAV-mxABE and the corresponding uninjected cochlea. (**E**) Deep sequencing results in the cochlea of *Myo6*$^{C442Y/C442Y}$ mice injected with AAV-mxABE and the corresponding uninjected cochlea. To compare the correction efficiency, paired Student's *t* test was used. *$P < 0.05$ and **$P < 0.01$.

S3B). Moreover, we designed primers (fig. S3C) to amplify the full length of mxABE from mouse cochlear complementary DNA (cDNA) and verify full-length mxABE expression in both left and right ears of some injected but not in the noninjected mice, consistent with the qRT-PCR results (fig. S3, D and E). Overall, mxABE could induce in vivo A-to-I conversion without substantial off-target edits.

In vivo treatment improves hearing function in *Myo6*^{C442Y} mice

To determine the therapeutic effect of the AAV-PHP.eB–mxABE-T activity on hearing function in *Myo6*$^{C442Y/+}$ mice, we performed recording of auditory brainstem response (ABR) and distortion product otoacoustic emissions (DPOAEs) across frequencies at 4, 8, 16, 24, and 32 kHz for treated and untreated ears at 9 and 12 weeks after injection (Fig. 3A and fig. S5, A and D). At 9 weeks, the ABR thresholds were significantly decreased at the frequency of 32 kHz in AAV-PHP.eB–mxABE-T–treated ears compared with the untreated ears (32 kHz: treated, 47.50 ± 7.68 dB, $n = 10$; untreated, 67.00 ± 4.36 dB, $n = 10$; $P < 0.01$) (Fig. 3B and figs. S4A and S5A). Furthermore, we also analyzed the DPOAE thresholds to detect the recovery of outer hair cells' (OHCs') amplification function (fig. S4B). Treated ears exhibited significantly decreased DPOAE threshold at 16 kHz compared with the untreated ears (16 kHz: treated, 38.57 ± 3.40 dB, $n = 7$; untreated, 57.14 ± 7.39 dB, $n = 7$; $P < 0.01$) (Fig. 3D and fig. S4B). In addition, the wave I latencies stimulated by 90-dB sound were shorter in the AAV-PHP.eB–mxABE-T–treated ears than untreated ones at 8 and 16 kHz, respectively (8 kHz: treated, 1.73 ± 0.08 ms, $n = 10$; untreated, 2.06 ± 0.09 ms, $n = 10$, $P < 0.05$; 16 kHz: treated, 1.57 ± 0.08 ms, $n = 10$; untreated, 1.92 ± 0.12 ms, $n = 10$, $P < 0.05$) (fig. S5B). We further detected an increase of wave I amplitudes after ABR analysis in the AAV-PHP.eB–mxABE-T–treated ears compared with the untreated ears at 9 weeks at 8-kHz but not at 16-kHz testing frequencies (8 kHz: treated, 2.05 ± 0.30 μV, $n = 10$; untreated, 1.09 ± 0.21 μV, $n = 10$; $P < 0.05$) (fig. S5C).

We observed that ABR thresholds at 12 weeks remained significantly decreased in treated ears compared to the untreated ones at 24 kHz (24 kHz: treated, 50.26 ± 5.04 dB, $n = 19$; untreated, 72.11 ± 4.70 dB, $n = 19$; $P < 0.001$) (Fig. 3C and figs. S4C and 5D). Furthermore, ABR thresholds at 8 kHz started showing improvement after the 12-week treatment. Compared with the untreated ears, a similar trend of significant lower DPOAE thresholds was detected as ABR results at 8 and 24 kHz after AAV-PHP.eB–mxABE-T injection (24 kHz: treated, 63.13 ± 6.88 dB, $n = 8$; untreated, 81.25 ± 2.06 dB, $n = 8$; $P < 0.05$) (Fig. 3E and fig. S4D). Consistent with decreased ABR and DPOAE threshold, wave I latency stimulated by 90-dB sound was shorter in the AAV-PHP.eB–mxABE-T–treated ears than untreated ones at 8 and 16 kHz (8 kHz: treated, 1.67 ± 0.05 ms, $n = 14$; untreated, 1.95 ± 0.09 ms, $n = 14$, $P < 0.05$; 16 kHz: treated, 1.58 ± 0.08 ms, $n = 14$; untreated, 1.89 ± 0.11 ms, $n = 14$, $P < 0.05$) (fig. S5E). The amplitude for the ABR test was found to be greater at 12 weeks after treatment at 8-kHz but not at 16-kHz testing

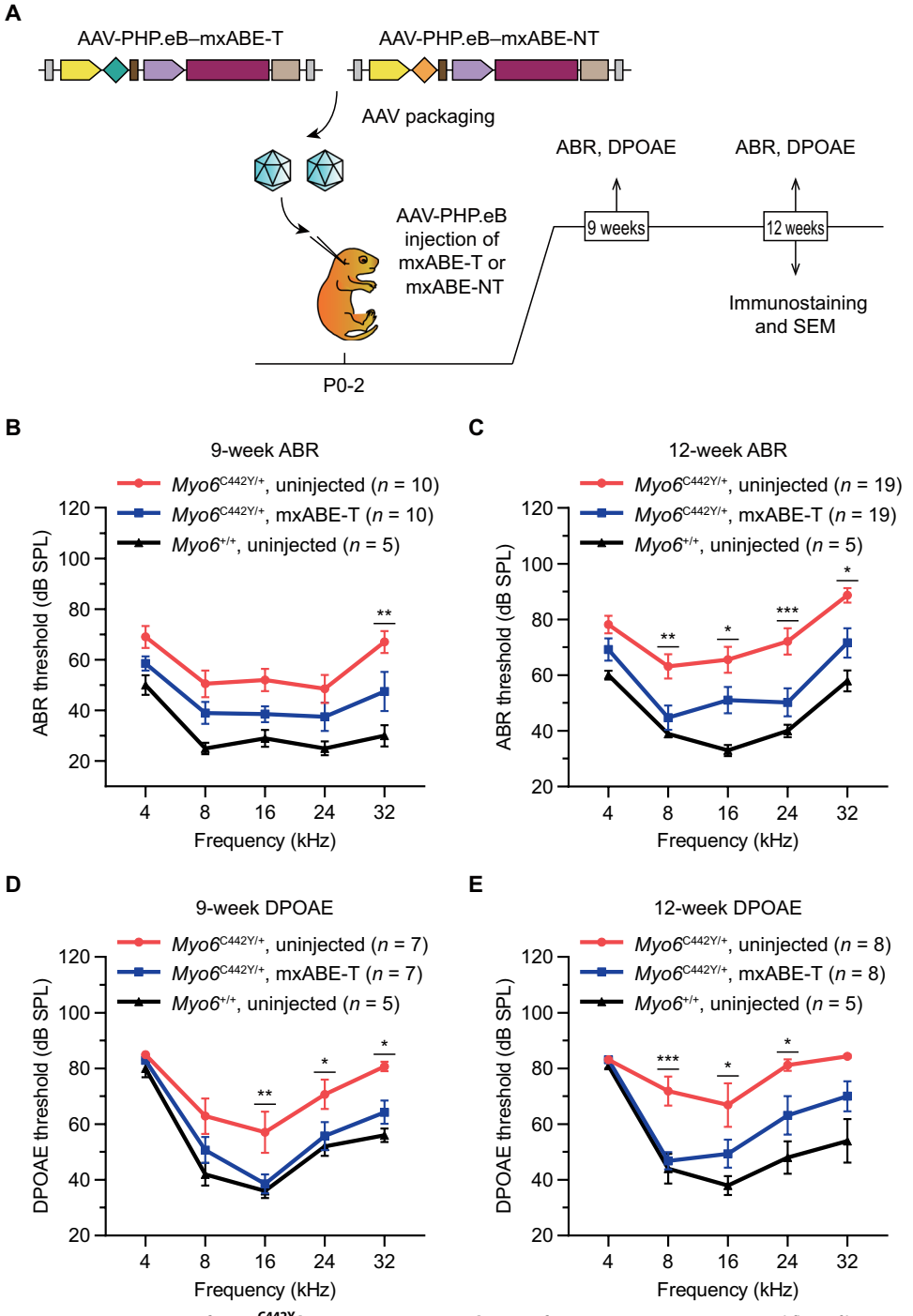

Fig. 3. In vivo correction of *Myo6*^{C442Y} by mxABE-T improves hearing function. (**A**) Diagrammatic workflow of hearing function analysis after AAV-mxABE therapy in *Myo6*$^{C442Y/+}$ mice. (**B** and **C**) ABR recovery results at 9 weeks (B) and 12 weeks (C) after treatment in the cochlea of *Myo6*$^{C442Y/+}$ mice injected with AAV-mxABE and the corresponding uninjected cochlea. *Myo6*$^{+/+}$ mice indicate WT mice without injection. SPL, sound pressure level. (**D** and **E**) DPOAE recovery results at 9 weeks after treatment in the cochlea of *Myo6*$^{C442Y/+}$ mice injected with AAV-mxABE and the corresponding uninjected cochlea. *Myo6*$^{+/+}$ mice indicate WT mice without injection. Data are presented as means ± SEM. Statistical tests were two-way ANOVA with Bonferroni correction for multiple comparisons. **P* < 0.05, ***P* < 0.01, and ****P* < 0.001.

frequencies (8 kHz: treated, 1.61 ± 0.34 μV, $n = 14$; untreated, 0.87 ± 0.12 μV, $n = 14$, $P < 0.05$) (fig. S5F), further supporting the rescue of hearing ability in disease mice.

In addition, all *Myo6*$^{C442Y/+}$ mice treated with AAV-PHP.eB carrying mxABE-v1 and nontargeting gRNA showed no improvement with ABRs and DPOAE profile similar to untreated *Myo6*$^{C442Y/+}$ mice (fig. S4, E and F), indicating that the phenotypic improvement of AAV-PHP.eB–mxABE-T–treated mice resulted from the specific correction of *Myo6*^{C442Y} RNA.

mxABE treatment increases survival rate of *Myo6*$^{C442Y/+}$ hair cells

Myo6$^{C442Y/+}$ mice exhibited substantial degeneration of OHCs as previously described (*24*). To assess the effect of RNA editing by AAV-PHP.eB–mxABE-T on hair cell survival, we counted the hair cells at 12 to 16 weeks. We found that the number of inner hair cells (IHCs) in *Myo6*$^{C442Y/+}$ mice was not different from that in either WT or AAV-PHP.eB–mxABE-T–treated ears (Fig. 4 and fig. S6). By contrast, there were more OHCs in the middle and basal turns of the cochlea in the AAV-PHP.eB–mxABE-T–treated ears (96.80 ± 2.92 cells and 68.60 ± 4.59 cells per 0.25 mm by 0.125 mm in the middle and basal turns of the cochlea, respectively; $n = 5$ mice) than in the untreated ears (83.60 ± 8.32 cells and 39.00 ± 10.86 cells per 0.25 mm by 0.125 mm in the middle and basal turns of the cochlea, respectively; $n = 5$ mice) (Fig. 4 and fig. S6). These results indicated that the survival rate of hair cells was improved by correction of *Myo6*^{C442Y} allele.

mxABE treatment prevents the degeneration of hair bundle morphology and preserves electrophysiological property

Stereocilia bundles on hair cells are responsible for sound detection, and morphological defects in the stereocilia can cause deafness. In our previous study (*24*), morphological abnormalities in cochlear hair bundles in *Myo6*$^{C442Y/+}$ mice were observed at 6 weeks. Most hair bundles anchored on the remaining OHCs and IHCs retained normal morphology, but some were disorganized, with fused stereocilia and rotated polarity. At 12 weeks, the number of hair bundles in WT mice was approximately twice that of the *Myo6*$^{C442Y/+}$ heterozygous mice along the middle and basal tonotopic axes (*26*). Thus, in the present study, the hair bundle morphology was evaluated by a scanning

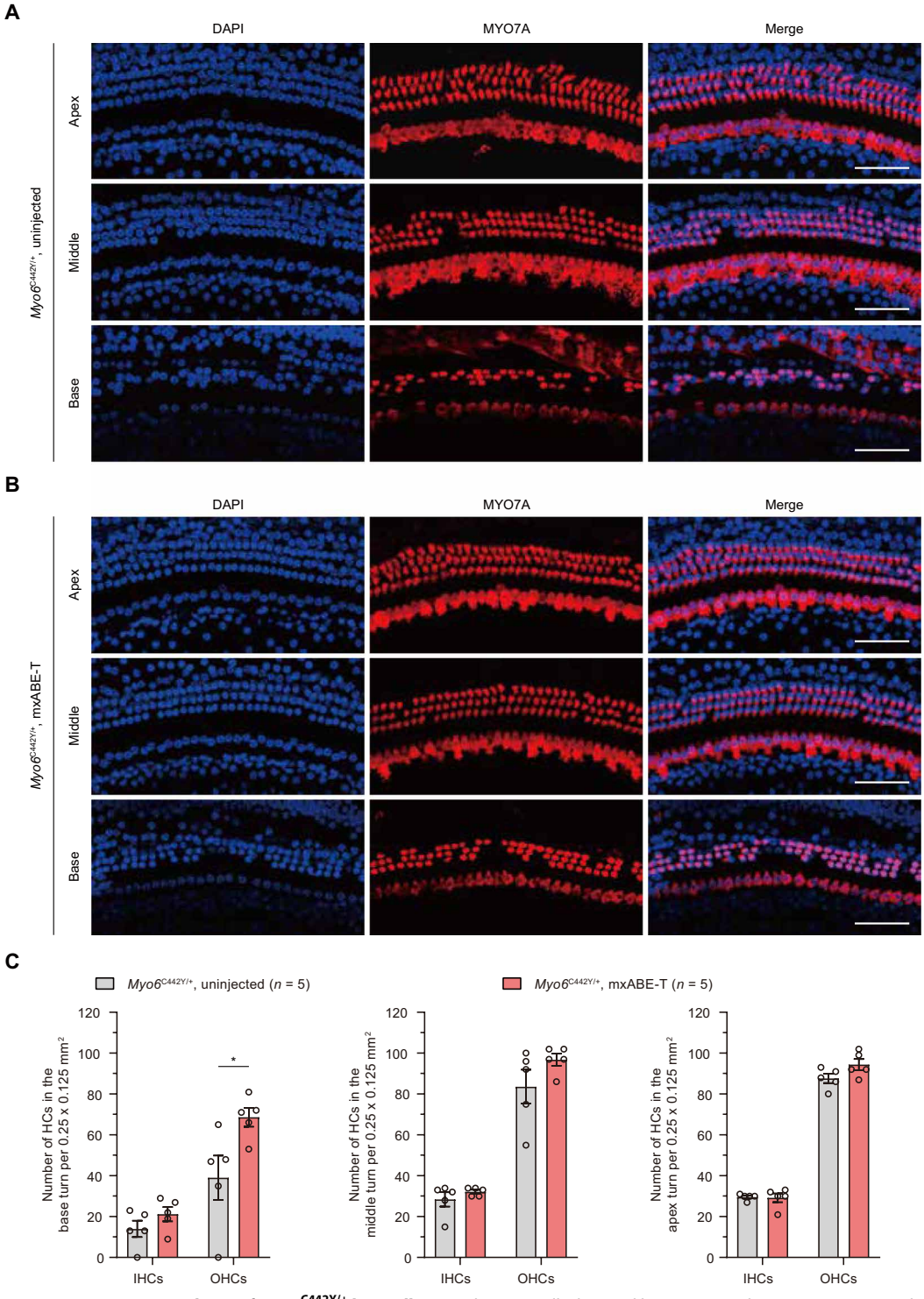

Fig. 4. mxABE-T treatment increases survival rate of *Myo6*$^{C442Y/+}$ hair cells. (**A** and **B**) Hair cells detected by MYO7A (red) immunostaining and DAPI (blue) for nuclei at the representative apex, middle, and basal turn of the cochlea between untreated (A) and mxABE-T–treated (B) *Myo6*$^{C442Y/+}$ mice. (**C**) Inner hair cell (IHC) and outer hair cell (OHC) numbers detected at the basal, middle, and apex turn of the cochlea between untreated and mxABE-T–treated *Myo6*$^{C442Y/+}$ mice, respectively. Data are presented as means ± SEM. To compare the means, unpaired Student's *t* test was used. *$P < 0.05$. Scale bars, 50 μm.

electron microscope in the AAV-PHP.eB–mxABE-T–treated and untreated ears of *Myo6*$^{C442Y/+}$ mice at 12 weeks of age (Fig. 5, A and B, and fig. S7). In WT control ears, the hair bundles were arranged into a normal pattern in OHCs and IHCs (Fig. 5, C and D). In *Myo6*$^{C442Y/+}$ mice, the surviving IHCs and OHCs showed substantial disorganization, with fused stereocilia and rotated polarity in some regions, consistent with our previous report (*24*). When AAV-PHP.eB–mxABE-T was delivered into the *Myo6*$^{C442Y/+}$ cochlea

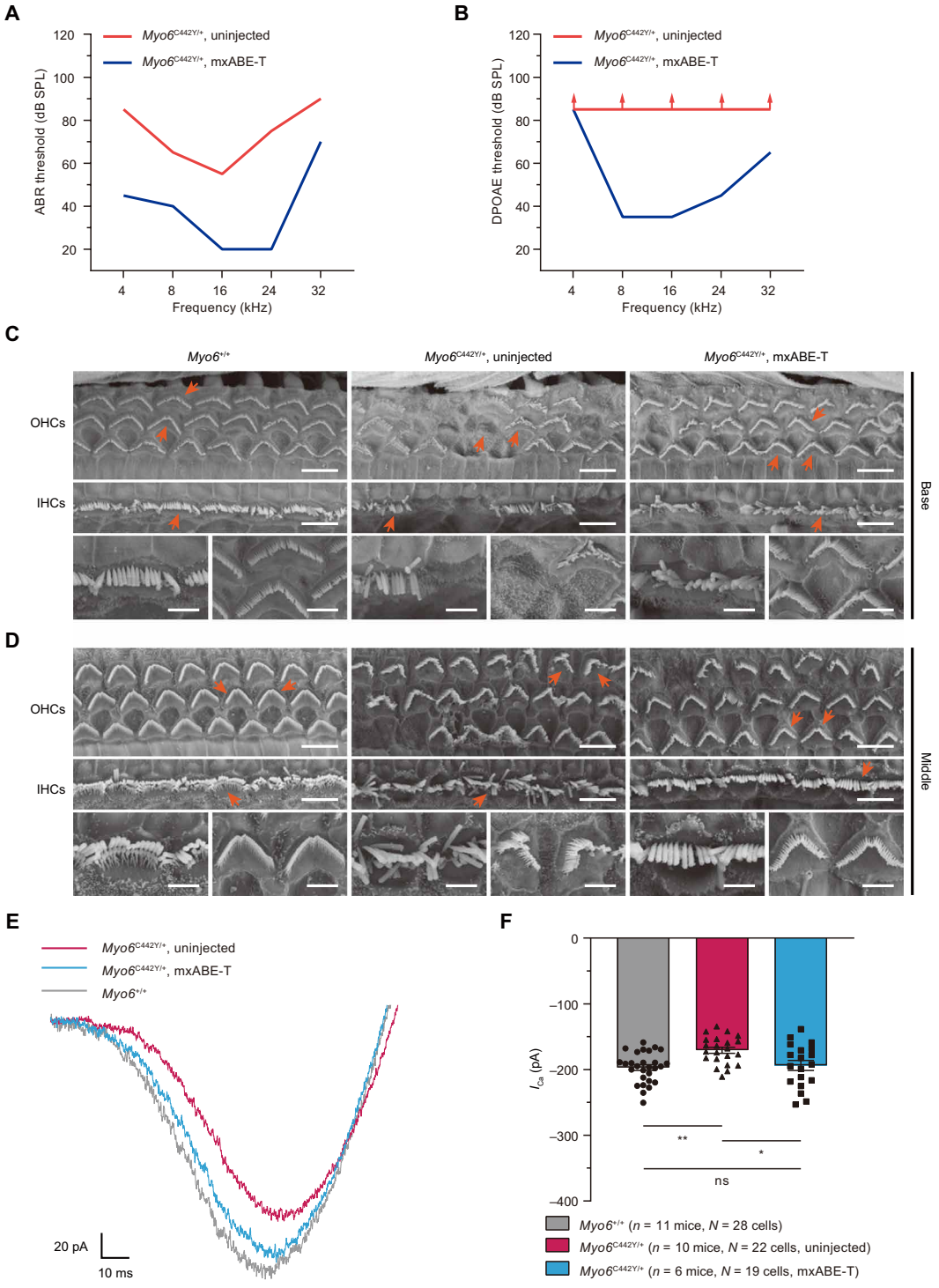

Fig. 5. mxABE-T treatment prevents the degeneration of hair bundle morphology in *Myo6*$^{C442Y/+}$ hair cells and preserves normal I_{Ca} amplitudes. (**A and B**) Representative ABR (A) and DPOAE (B) results in the cochlea of *Myo6*$^{C442Y/+}$ mouse injected with AAV-mxABE and the corresponding uninjected cochlea. Arrows indicate that the thresholds are higher than the maximal stimulus intensity tested. (**C** and **D**) Hair bundle morphology analyzed by a scanning electron microscope at the basal (C) and middle (D) turn of the cochlea among WT mice (*Myo6*$^{+/+}$), untreated mice, and mxABE-T–treated *Myo6*$^{C442Y/+}$ mice. Representative bundles (indicated by orange arrows) of OHCs and IHCs were enlarged in the third corresponding panel. (**E** and **F**) Electrophysiology analysis showed the recovery of IHC Ca^{2+} current amplitudes after treatment with AAV-PHP.eB–mxABE-T, representative I_{Ca} recordings in apical IHCs at P20 to P22 from untreated *Myo6*$^{C442Y/+}$ mice (red), WT mice (gray), and *Myo6*$^{C442Y/+}$ mice injected with AAV-PHP.eB–mxABE-T at P0 to P2 (cyan). Untreated *Myo6*$^{C442Y/+}$, −163.67 pA; treated *Myo6*$^{C442Y/+}$, −196.58 pA; WT, −206.70 pA (E). I_{Ca} values were recorded from a holding potential of −90 mV to +70 mV in 300 ms at P20 to P22 in IHCs from WT mice, uninjected *Myo6*$^{C442Y/+}$ mice, and mxABE-T–injected *Myo6*$^{C442Y/+}$ mice (F). Values and error bars presented as means ± SEM. To compare the means, statistical analysis was conducted with one-way ANOVA. *$P < 0.05$ and **$P < 0.01$. Scale bars, 5 μm (low-magnification figures) [top and middle panels of (C) and (D)] and 2 μm (high-magnification figures) [top and middle panels of (C) and (D)]. ns, not significant.

at P0 to P2, qualitative analysis showed more organized hair bundles in OHCs and IHCs (Fig. 5, C and D), which might help explain the functional recovery of the ABR and DPOAE performance. Although the degeneration of hair cells in the middle turns of the cochlea was mild in *Myo6*$^{C442Y/+}$ mice (Fig. 4), preserved hair cell morphology was observed in treated mice from the scanning electron microscope, in contrast to the obvious abnormalities in cochlear hair bundles of survival hair cells of untreated ear, which might be one of the reasons for mid-frequency hearing loss (Figs. 4 and 5A). Overall, the scanning electron microscope results indicated that hair bundle defects caused by *Myo6*$^{C442Y/+}$ mutation were amenable to restoration by injection of AAV-PHP.eB–mxABE-T.

Our previous studies have shown that the *Myo6*^{C442Y} mutation decreases Ca^{2+} current amplitude (I_{Ca}) without affecting whole-cell membrane capacitance (Cm) in IHCs, but our previous work observed no net increase in whole-cell membrane capacitance (ΔCm) in IHCs (*26*), indicating that the *Myo6*^{C442Y} mutation exerts no effect on the exocytosis of IHCs. Therefore, we explored whether the I_{Ca} in IHCs of *Myo6*$^{C442Y/+}$ mice was affected by AAV-PHP.eB–mxABE-T–mediated correction of the *Myo6*^{C442Y} transcript. The apical turn of the sensory epithelium was isolated directly from the *Myo6*$^{+/+}$ and AAV-PHP.eB–mxABE-T–treated and untreated *Myo6*$^{C442Y/+}$ cochleae at P20 to P22 for I_{Ca} analysis. We found that the *Myo6*^{C442Y} mutation resulted in decreased Ca^{2+} current amplitudes compared with WT *Myo6* mice (WT ears, −197.1 ± 4.4 pA, n = 11 mice, N = 28 cells; uninjected *Myo6*$^{C442Y/+}$ ears, −170.7 ± 4.5 pA, n = 10 mice, N = 22 cells), and the I_{Ca} of AAV-PHP.eB–mxABE-T–injected *Myo6*$^{C442Y/+}$ ears was recovered to −193.7 ± 7.6 pA (n = 6 mice, N = 19 cells) (Fig. 5, E and F).

DISCUSSION

Up to 60% of all genetic disorders are caused by point mutations (*27*). These can affect transcript stability, translation, or RNA splicing. Most point mutations lead to loss-of-function mutations, but gain-of-function mutations can be observed as well. There are 50% of sensorineural hearing impairment caused by genetic mutations in genes affecting different functions of hair cells. Our study shows that AAV-mediated in vivo delivery of mxABE-gRNA complex can achieve allele-specific correction of mutant RNA in the *Myo6*$^{C442Y/+}$ mouse model of a dominant inherited deafness, resulting in amelioration of hearing impairments. MYO6 plays an important role in maintaining the structural integrity of hair bundle for normal auditory function. Accordingly, we observed the rescue of both disorganized bundle morphology in OHCs at the basal turn of the cochlea and ABR for mxABE-treated *Myo6*$^{C442Y/+}$ mice, demonstrating effective therapeutic value of compact RNA base editors. Besides mxABE for A-to-I editing, we have previously developed a C-to-U RNA base editor from dCas13X, mxCBE, that potentially could correct C:G to T:A mutations found in genes such as *TMC1*, resulting in other forms of hearing impairments. Overall, the RNA base editing strategy developed in our study may inform the future development of RNA correction treatment for more genetic hearing loss disorders.

CRISPR-Cas9 systems can mediate targeted gene disruption or repair to treat different genetic diseases, including dominant-inherited and noninherited deafness (*26*, *28*–*30*). However, unintended repairing outcomes by CRISPR-Cas9 systems are permanent and often unpredictable and difficult to detect (*31*, *32*). In contrast to CRISPR-based DNA editing approaches, RNA editing events are transient and reversible in nature and only affect cells that express mutant RNA, therefore reducing the risk of long-lasting inadvertent side effects. In addition, DNA-targeting effectors such as Cas9 or Cas12 are often constrained by protospacer adjacent motif requirement that is nonobligated for RNA-targeting Cas13 protein. Some RNA-based therapeutics relying on ASO-mediated knockdown or splicing of aberrant RNA are already U.S. Food and Drug Administration (FDA)–approved, and their efficacy in targeting multiple cells or organs to restore genetic function has already been shown. Although RNA editing strategy was considered to be short-acting relative to genome-editing treatment, there are several critical factors in our strategy that might contribute to our successful rescue of hearing loss in disease mice. First, the highly infectious PHP.eB virus carrying mxABE ensured sufficient transduction of IHCs and OHCs for efficient RNA correction, confirming previous studies (*25*, *26*). Second, the administration of mxABE in the inner ears of neonatal mice via cochlear lateral wall has been previously reported to be safe (*28*, *33*, *34*).

High on-target and low off-target editing efficiency of RNA base editor played a crucial role in alleviating the hearing impairment after being delivered into hair cells. In our earlier study, the in vivo knocked out efficiency of *Myo6*^{C442Y} was 4.05%, on average, in *Myo6*$^{C442Y/+}$ mice by genome editing, which were from all the edited cells' genome in the whole cochlea (*26*). In this study, 4.22 ± 0.68% base editing efficiency for correction of mutant allele (*Myo6*^{C442Y}) to WT (*Myo6*$^{+}$) was detected at the mRNA level, which indicated the more real editing efficiency in vivo.

Our study provides scientific evidence for the potential of mxABE in treating deafness associated with G > A mutation. There are some limitations to be overcome before the safe and effective translation to the benefit of patients. First, our finding on the disparate editing efficiency of mxABE between in vitro and in vivo administration underscores the need to further improve in vivo editing efficiency for the *Myo6*^{C442Y} correction, which might be feasible via enhancing delivery and expression of mxABE in the cochlea. Second, it is important in the future to demonstrate the efficacy of mxABE in older or adult animals, which mimic the large population of noninfant patients found in the clinics. Moreover, the toxicity and immunogenicity profile of AAV-mxABE modality should be analyzed in a long-term study, although we currently observed no obvious toxicity of mxABE treatment in mice. Besides, we need to validate our approach for *Myo6*^{C442Y} correction with mxABE in human materials and adapt the AAV to human cells, i.e., induced pluripotent stem cell–based disease model. Overall, the translatability of AAV-mxABE should be further carefully evaluated in preclinical models. In summary, our results suggest that RNA base editing therapy has the potential for treatment of autosomal dominant hearing loss related to hair cell dysfunction and provide a complementary strategy to other approaches using RNA interference and DNA alterations.

MATERIALS AND METHODS

Study design

Our study aimed to demonstrate the efficacy of RNA base editing treatment for dominantly inherited hearing loss in the *Myo6*$^{C442Y/+}$ mouse model. Given the compact size and robust activity of mxABE shown in our previous research, we found that mxABE showed high

correction efficiency for *Myo6*^{C442Y} mutation with reporter assay in the HEK293T cell line. Therefore, we packaged the mxABE modality in AAV pseudotyped with PHP.eB capsid to deliver it into the cochlea of *Myo6*$^{C442Y/+}$ mice, resulting in the in vivo correction of *Myo6*^{C442Y} mutation and alleviation of progressive hearing loss in treated mice. Histological and functional characterization of treated versus untreated mice was performed with immunostaining of OHCs and IHCs in cochlea, ABR, and electrophysiology calcium recording. The cell line used in the study was indicated in the place of related results shown in the text, figure legends, and Materials and Methods. Animal size was chosen on the basis of the previous study in the field without statistical prediction. Animals were randomly assigned to the control and experimental groups, and researchers were not blinded to group information during the experiment and analysis. Details on the use of cell line and animal in different experiments could be found in the corresponding sections of Materials and Methods. Biological replicates were shown with the results in the figures and legends. Source data were provided in data file S1 or deposited in the public repository under accession number indicated in the Data and materials availability section.

Animals

Myo6 gene-modified mice (*Myo6*-C442Y) produced in the C57BL/6J strain were backcrossed with CBA/CaJ mice for more than 10 generations to obtain a homogeneous CBA/CaJ genetic background. Male and female *Myo6*-C442Y heterozygous mice were intercrossed to breed WT (*Myo6*$^{+/+}$), heterozygous (*Myo6*$^{C442Y/+}$), and homozygous (*Myo6*$^{C442Y/C442Y}$) progenies (*24*) used in this study. All mice used in this study were housed in a 12-hour light/12-hour dark cycle room with water and food ad libitum. All procedures were approved by the Institutional Animal Care and Use Committee of Fudan University, and we adhered to the National Institutes of Health (NIH) *Guide for the Care and Use of Laboratory Animals*.

Construction of plasmids

The *mCherry* and mouse *Myo VI* (c.G1325A)–fused expression cassette was cloned into Nhe I/Eco RV–digested pQQ156 backbone with the NEBuilder HiFi DNA Assembly Master Mix (New England Biolabs) as previously described (*16*). For target site gRNAs clone, briefly, oligos were synthesized and then annealed in a Bio-Rad thermocycler. Last, the annealed fragment was ligated into Bpi I–digested corresponding backbones using T4 DNA ligase (Thermo Fisher Scientific). All primers used in this study are provided in table S1.

AAV virus production

AAV-PHP.eB serotype (*25*, *35*) was used in this study. The mxABE plasmid with target or nontarget gRNA was sequenced before packaging into AAV-PHP.eB vehicle, and the AAV vectors were packaged by PackGene Biotech. The vector titer was 2.86×10^{13} and 3.99×10^{13} genome copies/ml as determined by qPCR specific for the inverted terminal repeat of the AAV-PHP.eB–*Myo6* and control virus.

Cell culture and transfection

The HEK293T cell line was cultured in Dulbecco's modified Eagle's medium (Gibco, reference no. 11965-092) supplemented with 10% fetal bovine serum (Gibco, reference no. 10099-141C), 1% Pen-Strep-Glutamine (100×) (Gibco, reference no. 10378-016), and 1% minimum essential medium nonessential amino acid (100×) (Gibco, reference no. 11140-050) in a humidified incubator at 37°C with 5% CO_2. Cells were passaged at a ratio of 1:5 every 3 days. For gRNA screening experiments, the HEK293T cell line was seeded in 12-well plates with 70% confluence, with the purpose of performing reporter and editor system plasmid transient transfection. Cells were cotransfected with 3.5 μg of vectors expressing *mCherry-Myo6* (c.G1325A) and editor in a ratio of 1:1 with Lipofectamine 3000 (Thermo Fisher Scientific) following the standard manufacturer manual.

Deep sequencing and total RNA-seq

After 2 days of transfection, for Sanger and deep sequencing, GFP-mCherry–positive cells were sorted by fluorescence-activated cell sorting (FACS) using BD FACSAria III or MoFlo XDP and lysed for RT-PCR. The total RNA was extracted from cells using TRIzol (Ambion) and then converted to cDNA using a reverse transcription kit (HiScript Q RT SuperMix for qPCR, Vazyme Biotech). The target region was amplified using the primers 5′-actacaccatcgtggaacag-3′ and 5′-ggcacagggatcctctca-3′ from cDNA with Phanta Max Super-Fidelity DNA Polymerase (Vazyme Biotech). Deep sequencing libraries were prepared with the Nextera XT DNA Library Prep Kit following the standard manufacturer manual and sequenced on a NovaSeq. Sequencing data were first demultiplexed by Cutadapt (v.2.8) (*36*) based on sample barcodes. The demultiplexed reads were then processed by CRISPResso2 (*37*) for the quantification of A-to-I conversion efficiency at target site. For transcriptome-wide RNA seq, HEK293T cells were cultured in 10-cm dishes with 70% confluence and cotransfected with 35 μg of plasmids to express *mCherry-Myo6* (c.G1325A) and/or editor with polyethylenimin (PEI). About 400,000 fluorescence-positive cells were collected by FACS, and RNA was extracted and then reverse-transcribed (RT) to cDNA, which was used for transcriptome-wide RNA-seq. An average of the three repeats is presented.

In vivo RNA editing analysis and qPCR

Temporal bones were harvested at 2 weeks from untreated *Myo6*$^{C442Y/+}$ mice or after AAV-PHP.eB–mxABE-T was injected into the right ear of mice, as previously described (*38*). Briefly, temporal bones were harvested after euthanizing the animal with inhaled CO_2, and the osseous spiral-shaped snail shells were removed carefully with microsurgical forceps under a dissection microscope. All soft tissues within the snail shell were collected including cochlear modiolus and transferred to TRIzol (Invitrogen). Then, total RNA was extracted from the organs of corti and RT using a reverse transcription kit (HiScript Q RT SuperMix for qPCR, Vazyme Biotech) according to the production protocol. The target region was amplified using the primers 5′-tctgccccatccctggaata-3′ and 5′-acccaggccctctttctgat-3′ from cDNA with Phanta Max Super-Fidelity DNA Polymerase (Vazyme Biotech). Deep sequencing libraries were prepared with the Nextera XT DNA Library Prep Kit following the standard manufacturer manual and sequenced on a HiSeq. Sequencing data were first demultiplexed by a custom python script based on sample barcodes. The demultiplexed reads were then processed by CRISPResso2 (*37*) for the quantification of A-to-I conversion efficiency at the target site. To quantify mxABE expression, qPCR analysis was conducted using AceQ qPCR SYBR Green Master Mix (Vazyme Biotech). The primers 5′-agatctgcttcggcagac-3′ and 5′-ggtacttcagctcgttcagg-3′ were used for amplification of *Cas13X.1* from mouse cochlear cDNA, and the primers 5′-tgtgtccgtcgtggatctga-3′ and 5′-ttgctgttgaagtcgcaggag-3′ were used for amplification of *Gapdh* as reference gene. Expression

was calculated by subtracting the respective housekeeping control (*Gapdh*) C_t values from the target C_t values to normalize for total input, resulting in ΔC_t values, and then the ΔC_t values of the right ear–injected mxABE *Myo6*$^{C442Y/+}$ mice or untreated *Myo6*$^{C442Y/+}$ mice were subtracted from the untreated *Myo6*$^{C442Y/+}$ mice's averaged ΔC_t value to obtain the respective $\Delta\Delta C_t$ values. Relative transcript abundance was computed as $2^{-\Delta\Delta Ct}$. All values were performed as biological replicates. To detect the full length of mxABE expression, the primers 5′-caccatggcccccaagaa-3′ and 5′-agtgggagtggcaccttc-3′ were used for PCR test.

RNA-seq analysis

The mRNA sequencing (high throughput) was performed using Illumina Genome Analyzer at Tiangen Biotech Co. Ltd., and the adapters were removed using Trimmomatic (v0.36) during sequencing. After quality control by FastQC, RNA-seq reads were trimmed by trim_galore to remove low-quality sequences as well as those with short lengths (less than 30). The high-quality reads were then analyzed to identify the editing sites using the pipeline of RADAR (RNA-editing analysis pipeline to decode all twelve types of RNA-editing events) (*39*) and presented as the mean of all repeats. Briefly, a two-round unique mapping strategy, implemented sequentially by hisat2 and BWA (Burrow-Wheeler Aligner)-MEM (maximal exact matches), was applied to capture alignments with flexible mismatches. The aligned reads with up to six mismatches were finally selected, and duplications were removed for variant calling using functions offered in Genome Analysis Toolkit. The alignments spanning introns were reformatted by SplitNCigarReads. Base quality was then recalibrated using BaseRecalibrator and ApplyBQSR, and single-nucleotide variants were called using HaplotypeCaller. The dbSNP (v.151) database downloaded from the National Center for Biotechnology Information, the 1000 Genomes Project (www.internationalgenome.org/), and the University of Washington Exome Sequencing Project (https://evs.gs.washington.edu/EVS/) were used to filter the sites that overlapped with common SNPs. The variants with less than 5 mutated or 15 nonmutated reads or an editing efficacy of less than 0.1 were further filtered. All data are available with the Sequence Read Archive (SRA) accession number PRJNA773257.

Inner ear injection

The inner ear injection method used in this study was the same as described earlier (*26*). With total injection volumes of 500 nl of mxABE-T or 358.4 nl of mxABE-NT virus per cochlea, about 1.43×10^{10} genomes were delivered into each ear of *Myo6*$^{C442Y/+}$ mouse pups at P0 to P2 with a rate of 3 nl/s. Briefly, pups were anesthetized by low-temperature exposure on ice for 1 min. Upon anesthesia, injections were made with a glass micropipette on a Nanoliter Microinjection System (World Precision Instruments) through the cochlear lateral wall after a post-auricular incision and exposure of the otic bulla and the stapedial artery under the operating microscope (*28*, *33*, *40*). After injection and skin suture, the pups were returned to their mother after they fully recovered. Standard postoperative care was applied after surgery.

Auditory testing

ABR measurements were recorded in a soundproof chamber using the RZ6 Acoustic System (Tucker-Davis Technologies). Briefly, mice of either sex were anesthetized by intraperitoneal injection of xylazine (10 mg/kg) and ketamine (100 mg/kg), and needle electrodes were inserted into the subcutaneous tissues of the vertex (the reference electrode), the mastoid portion (the recording electrode), and the rump of the animal (the ground electrode). Each animal was stimulated by 5-ms tone pips, and ABR potentials were evoked and subsequently amplified (10,000 times), filtered (300-Hz to 3-kHz passband), and averaged (1024 responses) at each sound intensity [decibel sound pressure level (SPL)]. Tone burst sound stimuli were presented at 4, 8, 16, 24, and 32 kHz to test the frequency-specific hearing thresholds. The threshold of a certain frequency was determined as the lowest SPL at which any ABR wave could be detected upon visual inspection and could be repeated. The amplitude of wave I of the ABR was measured from the peak of wave I to the following trough (*41*).

For DPOAEs, the f1 and f2 primary tones (f2/f1 = 1.2) were presented with f2 at 4, 8, 16, 24, and 32 kHz and L1-L2 = 10-dB SPL. For each f2/f1 primary pair, L2 was swept in 5-dB increments from 20- to 80-dB SPL. Waveform and spectral averaging were used at each sound intensity to increase the signal-to-noise ratio of the recorded ear canal sound pressure. DPOAE threshold was defined from the average spectra as the L2 producing a DPOAE of magnitude 5-dB SPL above the noise floor. The mean noise floor intensity was under 0-dB SPL across all frequencies (*29*, *30*).

During the whole procedure of acoustic testing, the mice were placed on a heating pad covered by a sterile gauze to maintain their body temperature. The animals were returned to the breeding center after they recovered from anesthesia and regained voluntary movement. In general, thresholds were defined by two independent observers. Data were analyzed and plotted using GraphPad Prism 8, and threshold means ± SEM are presented unless otherwise stated.

Electrophysiology analysis

Patch-clamp recording was performed in IHCs. As described previously (*26*, *42*), the apical turns of the cochlea were excised from both *Myo6*$^{+/+}$ and *Myo6*$^{C442Y/+}$ mice at P20 to P22 and then bathed in an oxygenated extracellular solution containing 123 mM NaCl, 5.8 mM KCl, 5 mM $CaCl_2$, 0.9 mM $MgCl_2$, 10 mM HEPES, 5.6 mM D-glucose, 0.7 mM $NaH_2PO_4{\cdot}H_2O$, and 2 mM Na-pyruvate [300 milliosmole per kilogram (mosm/kg), pH 7.40]. The tissue was visualized through a 60× water-immersion objective on an upright microscope (Olympus), and patch-clamp recordings were made through an EPC10 amplifier (HEKA Electronik, Lambrecht Pfalz, Germany) driven by the PATCHMASTER software (HEKA Electronik). Recording pipettes with a resistance of 5 to 6 megohms were coated with dental wax and then filled with an intracellular solution that contained 135 mM cesium methanesulfonate, 10 mM CsCl, 10 mM TEA-Cl, 2 mM EGTA, 10 mM Hepes, 3 mM Mg–adenosine 5′-triphosphate, and 0.5 mM Na–guanosine 5′-triphosphate (290 mosm/kg, pH 7.20). We applied a voltage ramp from a holding potential of −90 mV to +70 mV in 0.3 s and recorded the resulting Ca^{2+} current. All patch-clamp recordings were made at room temperature, and the liquid junction potential was corrected offline.

Immunostaining, confocal microscopy, and cell counting

For the in vivo experiments, the temporal bones of mice were harvested, cleaned, and fixed with 4% paraformaldehyde overnight at 4°C. After adequate decalcification in 10% EDTA, the entire sensory epithelium was dissected and preserved in phosphate-buffered saline (PBS) until staining. All samples were permeabilized and

blocked in PBS containing 1% Triton X-100 (1% PBS-T) and 10% donkey serum, respectively, at 4°C overnight. All primary antibodies were diluted in 1% PBS-T, and secondary antibodies were diluted in PBS. To observe hair cells, anti-MYO7A primary antibody (1:500 dilution; Proteus Biosciences, catalog no. 25-6790, RRID: AB_10015251) was used as the hair cell marker, appropriate Alexa Fluor–conjugated secondary antibody was used for detection, and 4′,6-diamidino-2-phenylindole (DAPI) was used to label the nuclei (1:800 dilution; Sigma-Aldrich, D9542). The fluorescent Z-stack images were visualized and collected using an Olympus FV3000 IX83 laser scanning confocal microscope and a ×40 objective. The maximum intensity projections of optical confocal sections are shown in the figures. ImageJ Fiji (NIH; https://imagej.net/software/fiji/) software was used to count the number of all the MYO7A-positive hair cells within a rectangular area of 0.25 mm by 0.125 mm, which contains the three rows of OHCs and one row of IHCs along the width direction. Adobe Illustrator CS6 was used for organizing figures.

Scanning electron microscope

The temporal bones of 12-week-old adult mice were harvested, and cleaned temporal bones were placed in 2.5% glutaraldehyde in 0.1 M PBS overnight at 4°C. After the samples were sufficiently decalcified in 10% EDTA, whole-mount tissues were dissected in sterile PBS buffer and then immersed in a 1% O_sO_4 solution in the dark for 4 hours. The samples were dehydrated with an ethanol gradient and a critical point dryer (Samdri-795, BioCryo Tousimis) according to the manufacturer's instructions. The mounted tissues were coated with a 10-nm layer of gold (JFC-1100), and an electron microscope (Hitachi S-4700 FESEM) was used for imaging (*24*, *26*).

Statistical analysis

All statistical values were presented as means ± SEM. Differences between datasets were considered to be significant at a P value of less than 0.05. Statistical analyses were conducted by two-way analysis of variance (ANOVA) with Bonferroni corrections for multiple comparisons for ABRs and DPOAEs and by one-way ANOVA for electrophysiology analyses. The unpaired two-tailed Student's t test was used for comparing means of latency, amplitude, and cell survival. The experiments were not randomized, and the investigators were not blinded to allocation during experiments and outcome assessment. GraphPad Prism (v 8.2.1) was used for statistics (www.graphpad.com/).

SUPPLEMENTARY MATERIALS

www.science.org/doi/10.1126/scitranslmed.abn0449
Figs. S1 to S7
Table S1
Data file S1
MDAR Reproducibility Checklist

View/request a protocol for this paper from *Bio-protocol*.

REFERENCES AND NOTES

1. H. M. Khosravi, M. F. Jantsch, Site-directed RNA editing: Recent advances and open challenges. *RNA Biol.* **18**, 41–50 (2021).
2. A. P. Gerber, W. Keller, RNA editing by base deamination: More enzymes, more targets, new mysteries. *Trends Biochem. Sci.* **26**, 376–384 (2001).
3. T. M. Woolf, J. M. Chase, D. T. Stinchcomb, Toward the therapeutic editing of mutated RNA sequences. *Proc. Natl. Acad. Sci.* **92**, 8298–8302 (1995).
4. M. Fukuda, H. Umeno, K. Nose, A. Nishitarumizu, R. Noguchi, H. Nakagawa, Construction of a guide-RNA for site-directed RNA mutagenesis utilising intracellular A-to-I RNA editing. *Sci. Rep.* **7**, 41478 (2017).
5. T. Merkle, S. Merz, P. Reautschnig, A. Blaha, Q. Li, P. Vogel, J. Wettengel, J. B. Li, T. Stafforst, Precise RNA editing by recruiting endogenous ADARs with antisense oligonucleotides. *Nat. Biotechnol.* **37**, 133–138 (2019).
6. L. Qu, Z. Yi, S. Zhu, C. Wang, Z. Cao, Z. Zhou, P. Yuan, Y. Yu, F. Tian, Z. Liu, Y. Bao, Y. Zhao, W. Wei, Programmable RNA editing by recruiting endogenous ADAR using engineered RNAs. *Nat. Biotechnol.* **37**, 1059–1069 (2019).
7. M. F. Montiel-Gonzalez, I. Vallecillo-Viejo, G. A. Yudowski, J. J. C. Rosenthal, Correction of mutations within the cystic fibrosis transmembrane conductance regulator by site-directed RNA editing. *Proc. Natl. Acad. Sci.* **110**, 18285–18290 (2013).
8. J. R. Sinnamon, S. Y. Kim, J. R. Fisk, Z. Song, H. Nakai, S. Jeng, S. K. McWeeney, G. Mandel, In vivo repair of a protein underlying a neurological disorder by programmable RNA editing. *Cell Rep.* **32**, 107878 (2020).
9. J. R. Sinnamon, S. Y. Kim, G. M. Corson, Z. Song, H. Nakai, J. P. Adelman, G. Mandel, Site-directed RNA repair of endogenous Mecp2 RNA in neurons. *Proc. Natl. Acad. Sci.* **114**, E9395–E9402 (2017).
10. S. Bhakta, M. T. A. Azad, T. Tsukahara, Genetic code restoration by artificial RNA editing of Ochre stop codon with ADAR1 deaminase. *Protein Eng. Des. Sel.* **31**, 471–478 (2018).
11. M. T. A. Azad, S. Bhakta, T. Tsukahara, Site-directed RNA editing by adenosine deaminase acting on RNA for correction of the genetic code in gene therapy. *Gene Ther.* **24**, 779–786 (2017).
12. P. Vogel, M. Moschref, Q. Li, T. Merkle, K. D. Selvasaravanan, J. B. Li, T. Stafforst, Efficient and precise editing of endogenous transcripts with SNAP-tagged ADARs. *Nat. Methods* **15**, 535–538 (2018).
13. I. C. Vallecillo-Viejo, N. Liscovitch-Brauer, M. F. Montiel-Gonzalez, E. Eisenberg, J. J. C. Rosenthal, Abundant off-target edits from site-directed RNA editing can be reduced by nuclear localization of the editing enzyme. *RNA Biol.* **15**, 104–114 (2018).
14. J. S. Gootenberg, O. O. Abudayyeh, B. Franklin, M. J. Kellner, J. Joung, F. Zhang, RNA editing with CRISPR-Cas13. *Science* **358**, 1019–1027 (2017).
15. O. O. Abudayyeh, J. S. Gootenberg, B. Franklin, J. Koob, M. J. Kellner, A. Ladha, J. Joung, P. Kirchgatterer, D. B. T. Cox, F. Zhang, A cytosine deaminase for programmable single-base RNA editing. *Science* **365**, 382–386 (2019).
16. C. Xu, Y. Zhou, Q. Xiao, B. He, G. Geng, Z. Wang, B. Cao, X. Dong, W. Bai, Y. Wang, X. Wang, D. Zhou, T. Yuan, X. Huo, J. Lai, H. Yang, Programmable RNA editing with compact CRISPR–Cas13 systems from uncultivated microbes. *Nat. Methods* **18**, 499–506 (2021).
17. S. Kannan, H. Altae-Tran, X. Jin, V. J. Madigan, R. Oshiro, K. S. Makarova, E. V. Koonin, F. Zhang, Compact RNA editors with small Cas13 proteins. *Nat. Biotechnol.* **40**, 194–197 (2022).
18. D. Katrekar, G. Chen, D. Meluzzi, A. Ganesh, A. Worlikar, Y. R. Shih, S. Varghese, P. Mali, In vivo RNA editing of point mutations via RNA-guided adenosine deaminases. *Nat. Methods* **16**, 239–242 (2019).
19. Z. M. Ahmed, R. J. Morell, S. Riazuddin, A. Gropman, S. Shaukat, M. M. Ahmad, S. A. Mohiddin, L. Fananapazir, R. C. Caruso, T. Husnain, S. N. Khan, S. Riazuddin, A. J. Griffith, T. B. Friedman, E. R. Wilcox, Mutations of MYO6 are associated with recessive deafness, DFNB37. *AM. J. Hum. Genet.* **72**, 1315–1322 (2003).
20. S. Melchionda, N. Ahituv, L. Bisceglia, T. Sobe, F. Glaser, R. Rabionet, M. L. Arbones, A. Notarangelo, E. Di Iorio, M. Carella, L. Zelante, X. Estivill, K. B. Avraham, P. Gasparini, MYO6, the human homologue of the gene responsible for deafness in Snell's waltzer mice, is mutated in autosomal dominant nonsyndromic hearing loss. *Am. J. Hum. Genet.* **69**, 635–640 (2001).
21. K. M. Sanggaard, K. W. Kjaer, H. Eiberg, G. Nürnberg, P. Nürnberg, K. Hoffman, H. Jensen, C. Sørum, N. D. Rendtorff, L. Tranebjaerg, A novel nonsense mutation in MYO6 is associated with progressive nonsyndromic hearing loss in a Danish DFNA22 family. *Am. J. Med. Genet. A* **146A**, 1017–1025 (2008).
22. T. Hasson, P. G. Gillespie, J. A. Garcia, R. B. MacDonald, Y. D. Zhao, A. G. Yee, M. S. Mooseker, D. P. Corey, Unconventional myosins in inner-ear sensory epithelia. *J. Cell Biol.* **137**, 1287–1307 (1997).
23. E. Mochizuki, K. Okumura, M. Ishikawa, S. Yoshimoto, J. Yamaguchi, Y. Seki, K. Wada, M. Yokohama, T. Ushiki, H. Tokano, R. Ishii, H. Shitara, C. Taya, K. Kitamura, H. Yonekawa, Y. Kikkawa, Phenotypic and expression analysis of a novel spontaneous myosin VI null mutant mouse. *Exp. Anim.* **59**, 57–71 (2010).
24. J. Wang, J. Shen, L. Guo, C. Cheng, R. Chai, Y. Shu, H. Li, A humanized mouse model, demonstrating progressive hearing loss caused by MYO6 p.C442Y, is inherited in a semi-dominant pattern. *Hear. Res.* **379**, 79–88 (2019).
25. X. Hu, J. Wang, X. Yao, Q. Xiao, Y. Xue, S. Wang, L. Shi, Y. Shu, H. Li, H. Yang, Screened AAV variants permit efficient transduction access to supporting cells and hair cells. *Cell Discov.* **5**, 49 (2019).
26. Y. Xue, X. Hu, D. Wang, D. Li, Y. Li, F. Wang, M. Huang, X. Gu, Z. Xu, J. Zhou, J. Wang, R. Chai, J. Shen, Z.-Y. Chen, G.-L. Li, H. Yang, H. Li, E. Zuo, Y. Shu, Gene editing in a Myo6 semi-dominant mouse model rescues auditory function. *Mol. Ther.* **30**, 105–118 (2022).
27. H. A. Rees, D. R. Liu, Base editing: Precision chemistry on the genome and transcriptome of living cells. *Nat. Rev. Genet.* **19**, 770–788 (2018).

28. X. Gao, Y. Tao, V. Lamas, M. Huang, W.-H. Yeh, B. Pan, Y.-J. Hu, J. H. Hu, D. B. Thompson, Y. Shu, Y. Li, H. Wang, S. Yang, Q. Xu, D. B. Polley, M. C. Liberman, W.-J. Kong, J. R. Holt, Z.-Y. Chen, D. R. Liu, Treatment of autosomal dominant hearing loss by in vivo delivery of genome editing agents. *Nature* **553**, 217–221 (2018).
29. X. Gu, D. Wang, Z. Xu, J. Wang, L. Guo, R. Chai, G. Li, Y. Shu, H. Li, Prevention of acquired sensorineural hearing loss in mice by in vivo Htra2 gene editing. *Genome Biol.* **22**, 86 (2021).
30. B. György, C. Nist-Lund, B. Pan, Y. Asai, K. D. Karavitaki, B. P. Kleinstiver, S. P. Garcia, M. P. Zaborowski, P. Solanes, S. Spataro, B. L. Schneider, J. K. Joung, G. S. G. Géléoc, J. R. Holt, D. P. Corey, Allele-specific gene editing prevents deafness in a model of dominant progressive hearing loss. *Nat. Med.* **25**, 1123–1130 (2019).
31. M. Kosicki, K. Tomberg, A. Bradley, Repair of double-strand breaks induced by CRISPR–Cas9 leads to large deletions and complex rearrangements. *Nat. Biotechnol.* **36**, 765–771 (2018).
32. H. Y. Shin, C. Wang, H. K. Lee, K. H. Yoo, X. Zeng, T. Kuhns, C. M. Yang, T. Mohr, C. Liu, L. Hennighausen, CRISPR/Cas9 targeting events cause complex deletions and insertions at 17 sites in the mouse genome. *Nat. Commun.* **8**, 15464 (2017).
33. Y. Shu, Y. Tao, Z. Wang, Y. Tang, H. Li, P. Dai, G. Gao, Z.-Y. Chen, Identification of adeno-associated viral vectors that target neonatal and adult mammalian inner ear cell subtypes. *Hum. Gene Ther.* **27**, 687–699 (2016).
34. Y. Wang, Y. Sun, Q. Chang, S. Ahmad, B. Zhou, Y. Kim, H. Li, X. Lin, Early postnatal virus inoculation into the scala media achieved extensive expression of exogenous green fluorescent protein in the inner ear and preserved auditory brainstem response thresholds. *J. Gene Med.* **15**, 123–133 (2013).
35. K. Y. Chan, M. J. Jang, B. B. Yoo, A. Greenbaum, N. Ravi, W. L. Wu, L. Sánchez-Guardado, C. Lois, S. K. Mazmanian, B. E. Deverman, V. Gradinaru, Engineered AAVs for efficient noninvasive gene delivery to the central and peripheral nervous systems. *Nat. Neurosci.* **20**, 1172–1179 (2017).
36. M. Martin, Cutadapt removes adapter sequences from high-throughput sequencing reads. *EMBnet.journal* **17**, 3 (2011).
37. K. Clement, H. Rees, M. C. Canver, J. M. Gehrke, R. Farouni, J. Y. Hsu, M. A. Cole, D. R. Liu, J. K. Joung, D. E. Bauer, L. Pinello, CRISPResso2 provides accurate and rapid genome editing sequence analysis. *Nat. Biotechnol.* **37**, 224–226 (2019).
38. C. A. Nist-Lund, B. Pan, A. Patterson, Y. Asai, T. Chen, W. Zhou, H. Zhu, S. Romero, J. Resnik, D. B. Polley, G. S. Géléoc, J. R. Holt, Improved TMC1 gene therapy restores hearing and balance in mice with genetic inner ear disorders. *Nat. Commun.* **10**, 236 (2019).
39. X. Wang, C. Ding, W. Yu, Y. Wang, S. He, B. Yang, Y.-C. Xiong, J. Wei, J. Li, J. Liang, Z. Lu, W. Zhu, J. Wu, Z. Zhou, X. Huang, Z. Liu, L. Yang, J. Chen, Cas12a base editors induce efficient and specific editing with low DNA damage response. *Cell Rep.* **31**, 107723 (2020).
40. L. A. Kilpatrick, Q. Li, J. Yang, J. C. Goddard, D. M. Fekete, H. Lang, Adeno-associated virus-mediated gene delivery into the scala media of the normal and deafened adult mouse ear. *Gene Ther.* **18**, 569–578 (2011).
41. N. F. Bramhall, C. E. Niemczak, S. D. Kampel, C. J. Billings, G. P. McMillan, Evoked potentials reveal noise exposure–related central auditory changes despite normal audiograms. *Am. J. Audiol.* **29**, 152–164 (2020).
42. H. Liu, J. Lu, Z. Wang, L. Song, X. Wang, G.-L. Li, H. Wu, Functional alteration of ribbon synapses in inner hair cells by noise exposure causing hidden hearing loss. *Neurosci. Lett.* **707**, 134268 (2019).

Acknowledgments: We thank the Core Facilities of CEBSIT (ION): the Optical Imaging facility (Y. Wang, Y. Zhang, and Q. Hu) and the FACS facility (H. Wu and L. Quan). We also thank Y. Sun, Z. Luo, and Z. Liu [principal investigator at the CEBSIT (ION)] for technical assistance. **Funding:** This work was supported by the Chinese National Science and Technology major project R&D Program of China (2018YFC2000101 to H.Y.), the Strategic Priority Research Program of Chinese Academy of Science (XDB32060000 to H.Y.), the National Natural Science Foundation of China (31871502 to H.Y., 31901047 to H.Y., 31925016 to H.Y., 91957122 to H. Y., 82021001 to H.Y., and 31922048 to C.X.), the Basic Frontier Scientific Research Program of Chinese Academy of Sciences From 0 to 1 original innovation project (ZDBS-LYSM001 to H.Y.), the Shanghai Municipal Science and Technology Major Project (2018SHZDZX05 to H.Y.), the Shanghai City Committee of Science and Technology Project (18411953700 to H.Y., 18JC1410100 to H.Y., 19XD1424400 to H.Y., and 19YF1455100 to C.X.), National Key Research and Development Program of China grant 2020YFA0908201 (to Y.S.), the National Natural Science Foundation of China (81822011 to Y.S., 82171148 to Y.S., 81771013 to Y.S., and 82171141 to G.-L.L.), and the Science and Technology Commission of Shanghai Municipality (21S11905100 to Y.S and 21JC401000 to G.-L.L.). **Author contributions:** Y.S., H.Y., H.L., C.X., and Q.X. jointly conceived the project and designed the experiments. Y.S., H.Y., H.L., and C.X. supervised the whole project. Q.X. designed vectors, performed in vitro experiments, scanned confocal imaging, and organized figures. Z.X. and Y.X. designed and performed experiments for in vivo virus injection, hearing function experiments, dissection of the cochlea, immunostaining, and scanning electron microscope experiments. Y.L. analyzed RNA-seq data. L.H. and S.H. assisted with immunostaining, hearing function experiments, and animal breeding. F.W., and G.-L.L. performed the electrophysiology experiments and analyzed the data. R.Z. and X.W. assisted with construction plasmids. Y.S., H.Y., and C.X. wrote the manuscript with data contributed by all authors who participated in the project. **Competing interests:** H.Y. is a founder of Hui-Gene Therapeutics. All other authors declare that they have no competing interests. **Data and materials availability:** All data associated with this study are present in the paper or the Supplementary Materials. RNA-seq data are available with the SRA accession number PRJNA773257.

Submitted 30 October 2021
Accepted 31 May 2022
Published 20 July 2022
10.1126/scitranslmed.abn0449

Science Translational Medicine

Rescue of autosomal dominant hearing loss by in vivo delivery of mini dCas13X-derived RNA base editor

Qingquan XiaoZhijiao XuYuanyuan XueChunlong XuLei HanYuanhua LiuFang WangRunze ZhangShuang HanXing WangGeng-Lin LiHuawei LiHui YangYilai Shu

Sci. Transl. Med., 14 (654), eabn0449. • DOI: 10.1126/scitranslmed.abn0449

Targeting the transcriptome

Targeting disease-relevant transcripts using RNA editing holds promise for treating genetic diseases, without the risks associated with permanent changes induced by DNA alterations. Here, Xiao *et al.* evaluated the therapeutic potential of a Cas13-derived RNA base editor for correcting a hearing loss–causing mutation in the myosin VI (*Myo6*) transcript in a mouse model. The RNA base editor composed of a Cas13X variant and the RNA editing enzyme adenosine deaminase was delivered in the cochlea of mice using an AAV. The treatment prevented hair cell loss and rescued auditory function in mice for up to 3 months after injection, suggesting that RNA editing might be effective for treating genetic disorders.

Science Translational Medicine (ISSN) is published by the American Association for the Advancement of Science. 1200 New York Avenue NW, Washington, DC 20005. The title *Science Translational Medicine* is a registered trademark of AAAS.